

1 **Contribution of Remote Sensing and GIS to mapping groundwater vulnerability in**
2 **arid zone: case from Amour Mountains- Algerian Saharan Atlas**

3
4 Rachid Kerzabi^{1,2,5}, Hamidi Mansour¹, Somia Yousfi^{2,5}, Ana Isabel Marín^{3,4}, Bartolomé
5 Andreo Navarro³, Kamar Eddine Bensefia⁵

6
7 ¹ University of Oran2 Ahmed Ben Bella, 31000 Oran, Algeria

8 ² Laboratory 25 «PRHPM-LE-CT», Department of Earth and Universe Sciences, Uni-
9 versity of Tlemcen 13000 Tlemcen, Algeria

10 ³ Department of Geology and Centre of Hydrogeology of the University of Málaga
11 (CEHIUMA), 29071 Málaga, Spain

12 ⁴ European Topic Centre of University of Malaga (ETC-UMA), 29071 Málaga, Spain

13 ⁵ Department of Earth and Universe Sciences, University of Tlemcen, 13000, Tlemcen,
14 Algeria

15
16 rachidkerza@gmail.com

17 **Abstract.** Protecting groundwater resource from pollution in arid zone is coming
18 an important act for sensing development in this region calling for geomatics tools
19 to characterize the geological and hydrogeological environment. The present work
20 gives a new way to combine remote sensing and geographic information systems
21 to elaborate groundwater vulnerability map of the aquifer namely Deffa watershed
22 (in Amour Montains). This region is a good example of arid zones how know an
23 important growth of agriculture, but there is under gap of geological, hydrogeolog-
24 ical and soil knowledge. Firstly, we analyzed the Landsat 8-OLI image data with
25 bands combination, ratios composition in RGB and filters to map the lithology's
26 contours and lineaments. The false color composition of bands (765, 753, and 543)
27 in RGB given the primary lithological delimitation. Supported by band rationing
28 technique, we produced of 1/50000 geological map. The filter treatments given the
29 lineament map superposed to the first one to realize geo-structural map. In addition,
30 these images were used to elaborate pedology map, using Decision Tree (Slope,
31 Redness Index and Lithology parameters). The resulting maps (lithology, lineament

32 and soil) and additional spatial information (aquifer type and deep of groundwater
33 surface and precipitations...) were combined by GIS to map the groundwater vul-
34 nerability indexes by GOD and PI methods. Both of maps displayed four classes of
35 vulnerability: between Low and Extreme in the first map, and Very low to High
36 vulnerability in the second one. In the some areas, we have controversial values of
37 vulnerability; this leads us to validate these maps using pollutions indicators (NO_3^-
38 , NH_4^+ and SO_4^{2-}). The validation tools applied allowed to discriminate that the PI
39 results are consistent with the spatial and temporal patterns of pollutants.

40

41 **Keywords:** Groundwater, Vulnerability, Remote sensing, GIS, Arid zone.

42

43 **1 Introduction**

44 The protection of groundwater resource from pollution in arid zone is a challenge, espe-
45 cially when the geological and hydrogeological conditions favorite immigration of pollu-
46 tants. In arid and semi-arid countries with faster urbanization, and development of agri-
47 cultural areas and intensification, the assessment of vulnerability of groundwater aims to
48 be a tool for the decisionmakers and land planner since this allow to identify the most
49 vulnerable zones and supports the sustainable water resources management (Secund et
50 al., 1998; Saidi et al., 2011; Qian et al., 2012; Thomas and Duraisamy, 2018). The ground-
51 water vulnerability mapping is one of the most applied tools to analyses the sensitivity of
52 aquifers to pollution. However, to map efficiently the vulnerability to pollution requires
53 a great deal of detailed information about surface and subsurface conditions. Furthermore,
54 spatially explicit information is necessary, the scale of which must be sufficiently detailed
55 to obtain reliable and accurate cartography.

56 Remote sensing (RS) is an ideal approach for detailed mapping of terrain features and
57 surface structure and, thank to the several platforms, such as Copernicus Land Monitoring
58 Service or XXX for accessing to free satellite imagery, this is an efficient tool for land
59 monitoring (Zumsprekel and Prinz, 2000, Gomes et al., 2005, Zoheir and Emam,
60 2012, Van der Meer et al., 2012, Pournamdary et al., 2014a, Pournamdary et al.,
61 2014b, Gabr et al., 2015, Eldosouky et al., 2017, Beiranvand et al. 2018, Bentaher and

62 Raji, 2020). Multispectral data is able to provide information on lithology or rock com-
63 position based on spectral reflectance (Ridwan et al, 2018).

64 There are relevant gaps of knowledge and datasets for the study area of this work,
65 Amour Mountains, central portion of Algerian Saharan Atlas. One of the most basic lack
66 of information is a digital lithologic information at proper scale that allows going in depth
67 in the hydrogeological study and the further groundwater protection. Under this frame-
68 work, this work aims to produce a lithological map at 1/50000, covering the extend of the
69 study area, by the treatment and interpretation of satellite images of Landsat OLI-8, to
70 rectify the lithological contours and elaborate the lineament and soil maps is the first step
71 of this work. These maps will contribute to the overall knowledge and the digital database
72 available about Amour Mountains to enrich the scientific community.

73 Additionally, second part of this paper presents the groundwater vulnerability map to pol-
74 lution calculated by GOD (Foster et al, 2007) and PI (Goldscheider et al, 2000) methods
75 as example of use the digital maps produced under this work and as first approaches to
76 protect the groundwater resource of this aquifer in arid zone. Vulnerability maps from
77 both methods are discussed and validated, to check which approach present better protec-
78 tion of groundwater resources in arid zone.

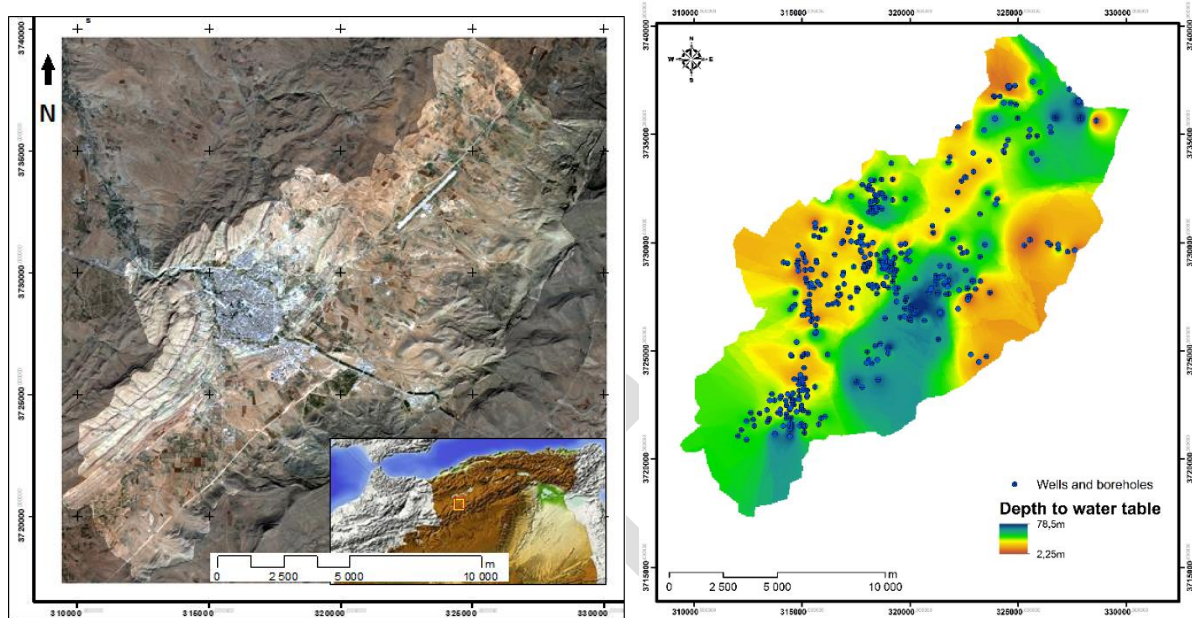
79

80 **2 Materials and Methods**

81 The study zone is the Deffa catchment, that covers an area of 208.85 km², is part of Amour
82 Mountains. Study catchment is a longue depression-oriented SW-NE surrounded by
83 many mountains peaks (Fig. 1). In terms of geology, the formations comprise the Tertiary
84 and Quaternary continental deposits, the outcrops range from the lower Callovian to the
85 Berremian-Aptian-Albian. From morphology point of view, the main features are anti-
86 clines formed by sandstone-clay and carbonate series, from the Jurassic and the Creta-
87 ceous. The Cretaceous outcrops correspond to the less accentuated reliefs (Cornet, 1952).
88 Hydrogeologically, the Infra-Cretaceous, Berremian-Aptian-Albian sandstones, Tertiary
89 and Quaternary sediments form the major aquifer systems of the study site. The absence
90 of impermeable layers causes hydraulic continuity conditions of all aquifers series. This
91 multilayer aquifer is exploited by 400 wells and drillings (B.E.T.G.H, 2003). This valua-
92 ble information served to estimate the groundwater level map based on the interpolation

4

93 of the well static water levels using the GIS tool inverse distance weighted method (Fig.
94 2).



95

96 **Fig. 1. Geographic situation of study region**

97 **Fig 2. Depth to water table in Deffa catchment**

98 Landsat 8-OLI images were acquired on third of December 2018. It has a nominal cen-
99 ter path of 196 and row of 37 according to the Worldwide Reference System. From eleven
100 bands available in the USGS Earth Explorer website (USGS, 2019), just seven first one
101 (30 m of resolution) was used to the deferent pretreatment (radiometric calibration and
102 atmospheric correction) and treatment (combination of bands, ration and filter). Different
103 techniques were applied in band Image stacking: RGB composites, bands ratios, Vegeta-
104 tion and Soil indexes and Decision Tree for geo-structural, land occupation and soil maps.
105 These were supportive to image interpretation and vulnerability mapping in GIS (Fig. 3).
106 Differentiation and delimitation of rock types is done by creating color composite images;
107 Standard bands combination such as 765 in RGB was prepared also band-rationing tech-
108 nique is used to detect outcrops limits in bare ground. The aridity of study zone made the
109 rectification of geological limits easy due to the absence of vegetation cover. Addition-
110 ally, different filters (0, 45°, 90° and 135°) helped us to elaborate lineament map. Both
111 maps derived from images at 30m spatial resolution, being the derived maps at scale 1/50
112 000.

113 The NDVI (Normalized Difference Vegetation Index) (Jensen, 1996) give an idea of
114 vegetation cover in study area.

115 On the other hand, there was an important lack of information regarding the pedological
116 map. The strength of the relationships between soils properties and environmental varia-
117 bles (slope, RI (Madeira, 1993) and geological nature) were used to implement the Deci-
118 sion Tree (DT) (Fig. 4) for discriminate different soil types and outline a soil map. This
119 prediction classification is frequently used to digital soil mapper (Hash, 2008; Moonjun
120 et al, 2008; Engle et al, 2010). The DT algorithm was formulated based on the Raster
121 calculating tools (if, then, else): slope, RI and lithology considered like nodes, controlled
122 by conditions used by some authors.

123 After that, these maps were transferred to GIS. The details given by RS treatment (maps
124 of lithology and lineament in 1/50 000) were combined with the information of geo-struc-
125 tural map (1/200000) in order to create the fracturing and lithological maps.

126 The digital terrain model was downloaded from (USGS, 2019) served to delimit the
127 watershed of Deffa and establish topography map using GIS. Then, in GIS we created a
128 database including all maps and data from bibliography (groundwater confinement factor,
129 depth to groundwater, nature of vadose zone, precipitation). This constitutes the database
130 to estimate the groundwater vulnerability maps by the application of GOD and PI meth-
131 ods.

132 The GOD method, because of its simplicity of concept and application, it is the first
133 method used in this work. The GOD vulnerability index (Foster, 1987; Foster and Hirata,
134 1988) characterizes aquifer pollution vulnerability based on the following (generally
135 available or readily determined) parameters (Foster et al, 2007):

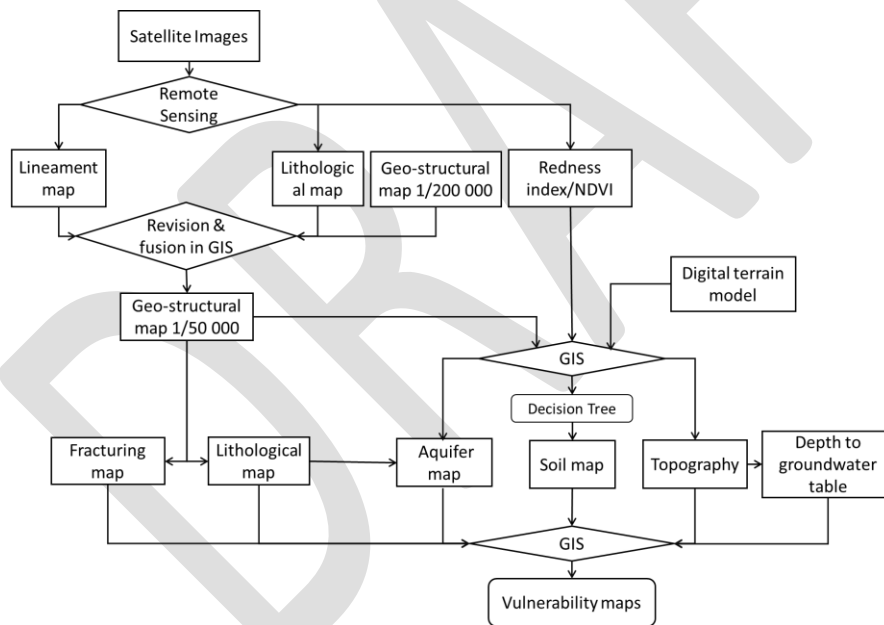
- 136 ● Groundwater hydraulic confinement, in the aquifer under consideration.
- 137 ● Overlying strata (vadose zone or confining beds), in terms of lithological character
138 and degree of consolidation that determine their contaminant attenuation capacity
- 139 ● Depth to groundwater table or to groundwater strike in confined aquifers.

140 For more precision, the PI method is used to estimate vulnerability index taking account
141 more parameters (infiltration, soil...). It is based on two factors; protective cover (P fac-
142 tor) and the infiltration conditions (I factor) (Goldscheider, 2003). The protective cover
143 results from the thickness and hydraulic conductivity of all the strata between the ground

144 surface and the groundwater table (including soil, subsoil and unsaturated zone). The I
 145 factor indicates the degree to which the protective cover is bypassed as a result of surface
 146 and near-surface concentration of flow. The protection factor π is obtained by multiplica-
 147 tion of P and I. More details about PI can be found in (Goldscheider et al, 2000).

148 Validation of groundwater vulnerability maps can be performed by several ways (Ma-
 149 rín et al. 2015). Among the methods the comparison of the vulnerability index/map with
 150 water quality parameters are the most used with confident results (Ghazav and Ebrahim,
 151 2015). To validate vulnerability maps, we used the pollution indicators concentrations in
 152 groundwater from water analyses: NO_3^- of 56 boreholes and SO_4^{2-} and NH_4^+ of just 17
 153 one (ADE, Algerienne Des Eaux 2018-2019). The concentrations of these elements in the
 154 groundwater collected of these boreholes are compared with both of GOD and PI maps.
 155 Nevertheless, just nitrate concentration was chosen for correlation study.

156



157

158 **Fig. 3. Deferent steps of data treatments.**

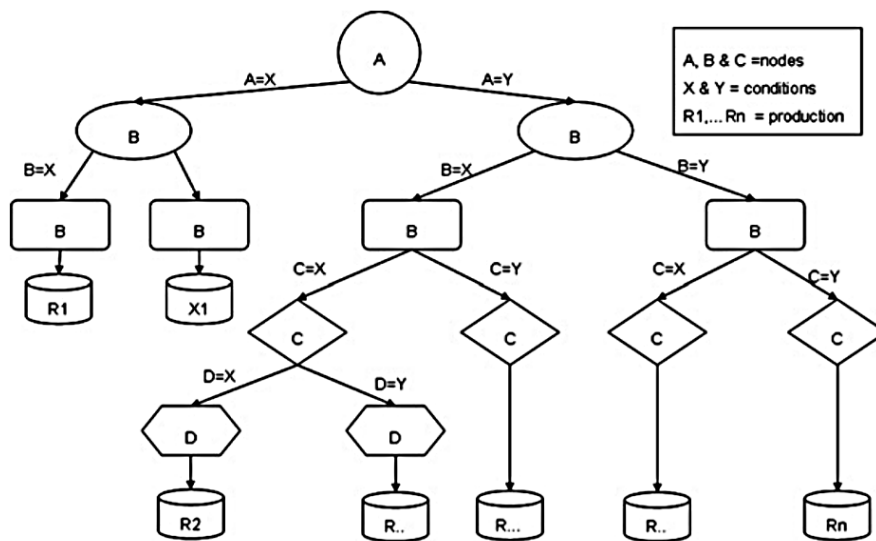


Fig. 4. The exemplifier of a simple decision tree structure (Moonjun et al, 2010)

3 Results

3.1 Remote sensing treatment

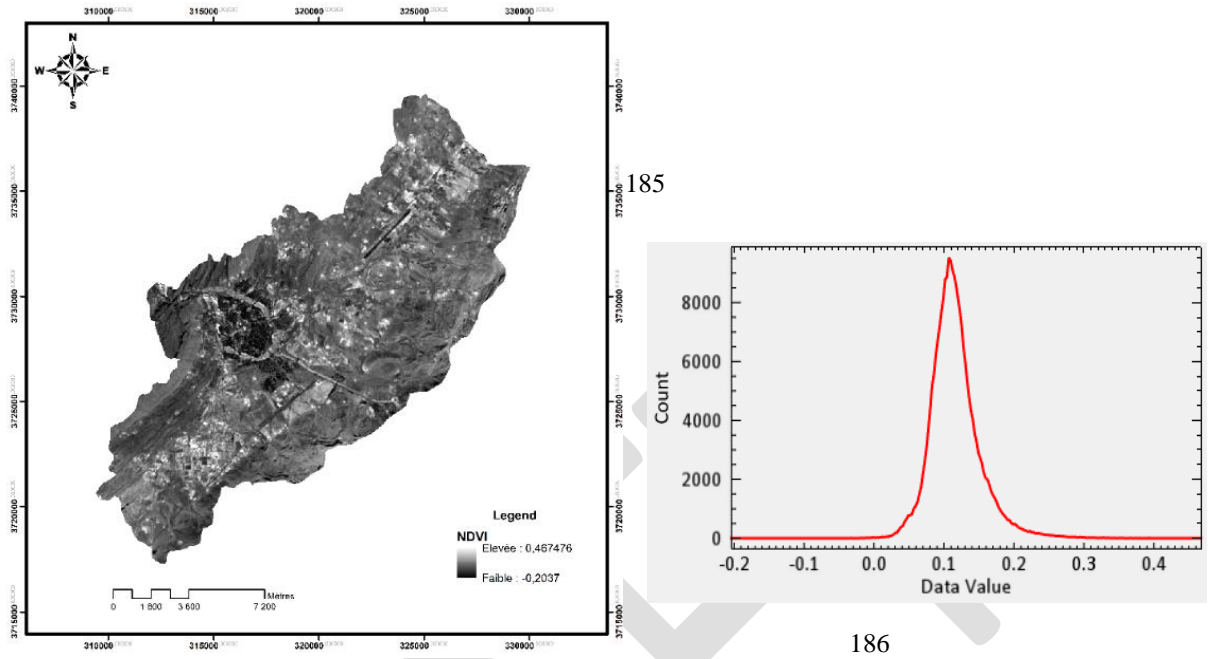
In this study, we used RS treatment to identify the lithology, lineament network and soil nature, in Deffa watershed. Prior to attempting the different classifications, the pre-treatment (radiometric correction and atmospheric correction) was performed to achieve reflectance data. NDVI is considered in many studies (Martiny et al, 2006; Guerrero et al, 2016, Kazi Tani, 2016; Yadav and Borana, 2019) like a significant parameter to mapping land occupation in arid zone; in figure 5a, NDVI presented a low value, between -0.2 and 0.45. In the histogram of NDVI (Fig. 5b), the values have a “Bell Curve” at 0.1, more than 32% of study surface is in this first class (<0.1). Between 0.1 and 0.3, we have 67.7%: degraded or absence of vegetation cover. Just 0.1% present high value of NDVI (>0.3-0.45) indicate a considerable vegetation cover.

For the first category of analyses, the important results that we based to classify the lithology are color composite (765, 753 and 543) (Fig. 6) and ratios assembling in RGB: (6/7, 6/4, 6/5) (6/7, 4/2, 5/4) and (7/6, 5/6, 2/4) (Fig. 7). To elaborate the lineament map, we used four filter with directions: 0, 45°, 90° and 135°. The assembly of filter results is show in figure 8a. The lineaments rosacea is presented in figure 8b.

The validation of lithology and lineament network were doing in GIS. The figure 9 present the geo-structural map of Deffa watershed.

181

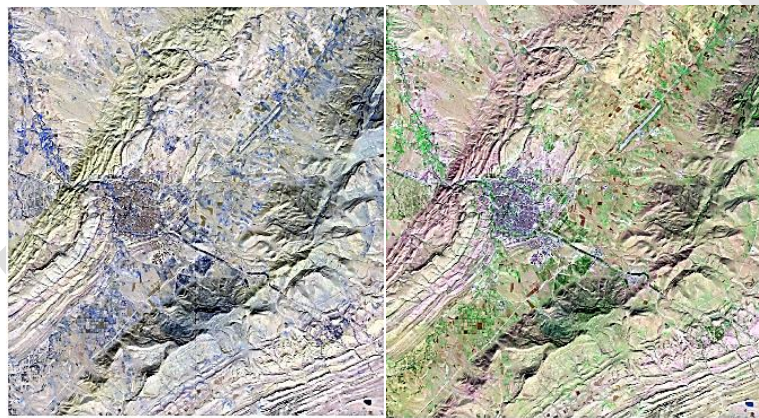
8



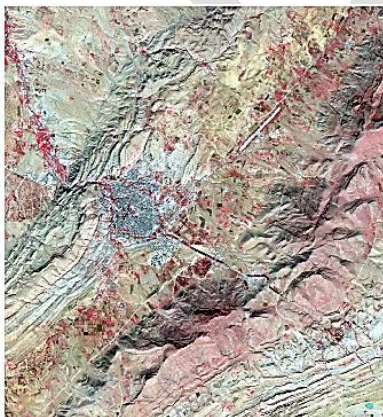
187
188

a. b.
Fig. 5: (a) NDVI image and (b) histogram of the study region.

189

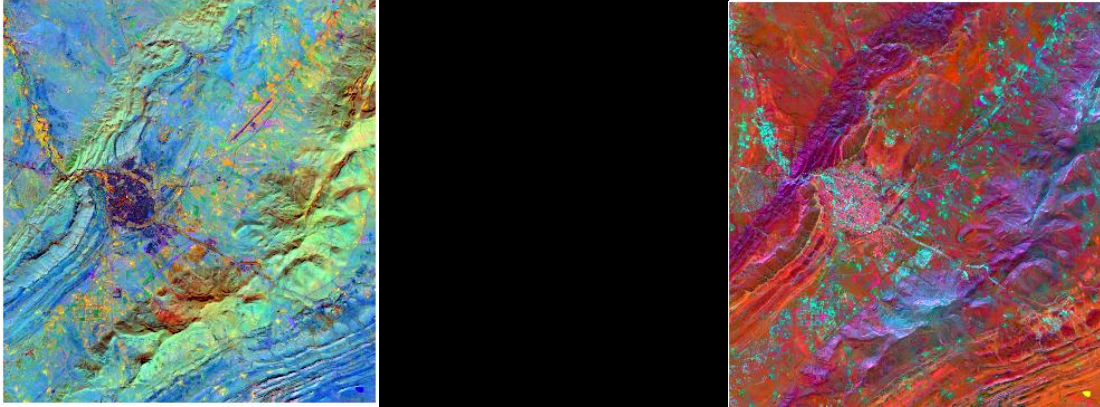


190

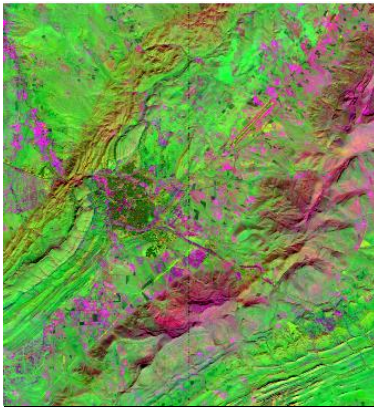


191

Fig. 6. Landsat 8-OLI color composite image, RGB=765, 753, 543.



192



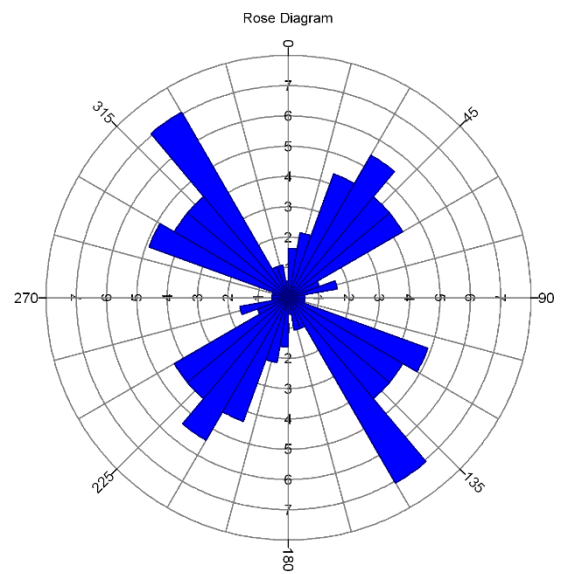
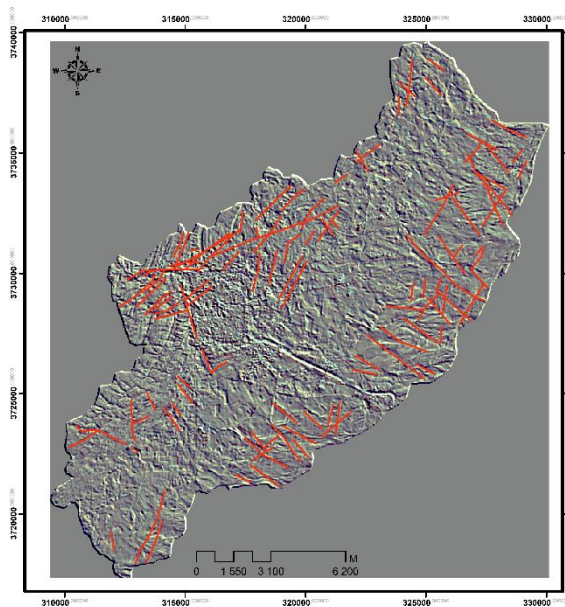
193

194

Fig. 7. Landsat 8-OLI bands ratios assembling in RGB: (6/7, 6/4, 6/5) (6/7, 4/2, 5/4) and (7/6, 5/6,

195

2/4).



196

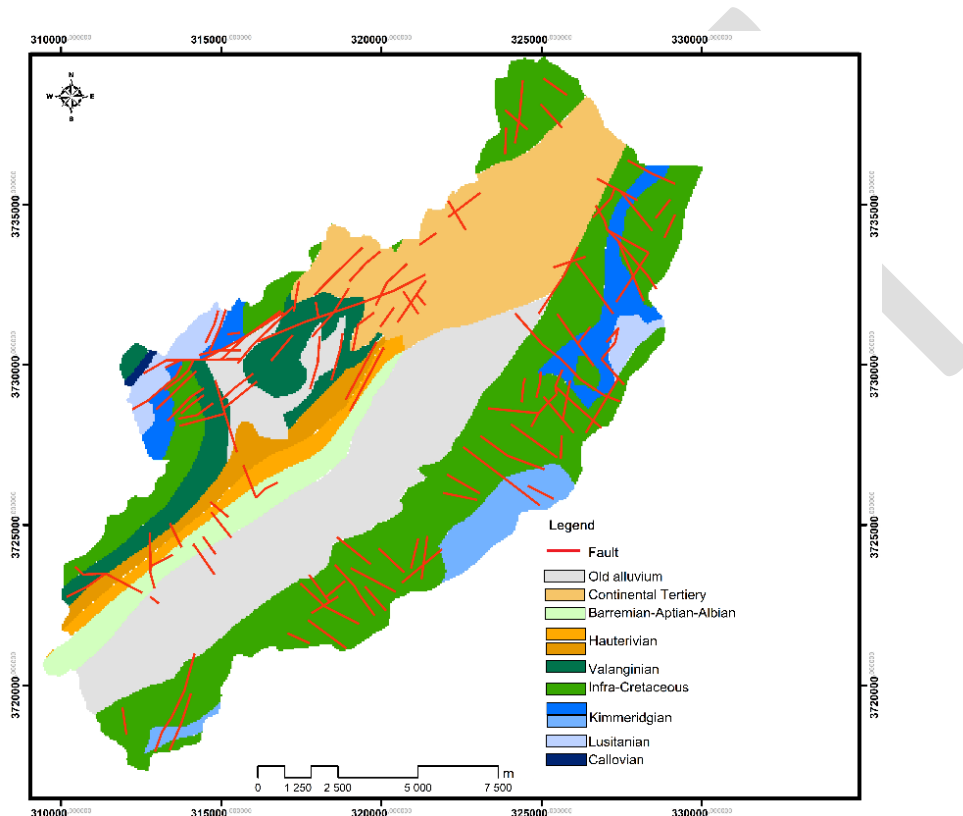
197

10

198 **Fig. 8. (a) Landsat 8 OLI filter (135°) with network lineament, (b) rosacea of results lineament**

199

200 The second category of RS treatment concerned pedology classification. For that, we
201 calculated the RI (Fig. 10) and integrated it in DT with slope and lithology parameters
202 (Fig. 11). The results were four classes of soil and land occupation (Fig. 12): Lithosols,
203 Poorly Developed Soil (P. D. Soil), Calcisols and Fersialsols.
204



205

206 **Fig. 9 Geo-structural map fusion all data in GIS.**

207

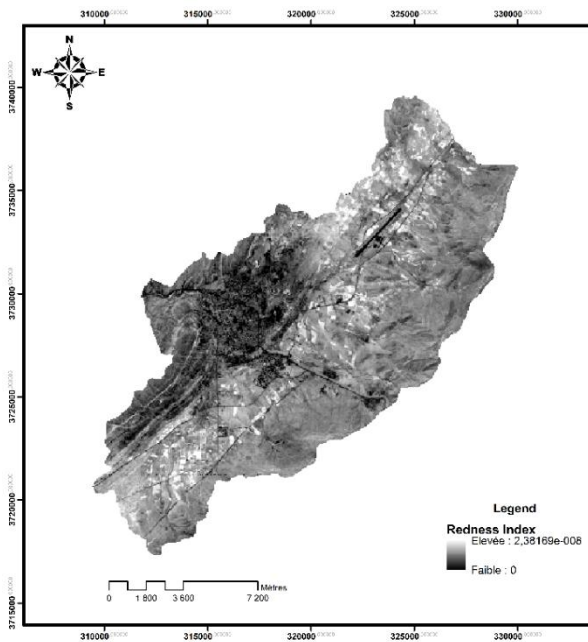
208 **3.2 GIS and vulnerability indexes**

209 The second step involved the generation of a GIS database to compile all relevant datasets
210 that are input data for assessing the vulnerability of groundwater to the pollution accord-
211 ing to GOD and PI methods (Foster et al, 2007; Goldscheider et al, 2000). These include
212 the spatial RS products and field datasets.

213

214 **3.3 GOD map**

215 Groundwater confinement, Overlying strata and Depth to groundwater table construed
 216 three layers used to mapping GOD index (Fig. 13). The geo-structural map result of RS,
 217 served to elaborate O layer, identifying lithological character and degree of consolidation
 218 of unsaturated zone or confining beds. This approach displayed four classes of vulnera-
 219 bility, between low and extreme, which occupied most of basin surface, mainly in bound-
 220 aries of the basin.
 221



231

232 **Fig. 10. Image of Redness index of the study area.**
 233 **treatment in**

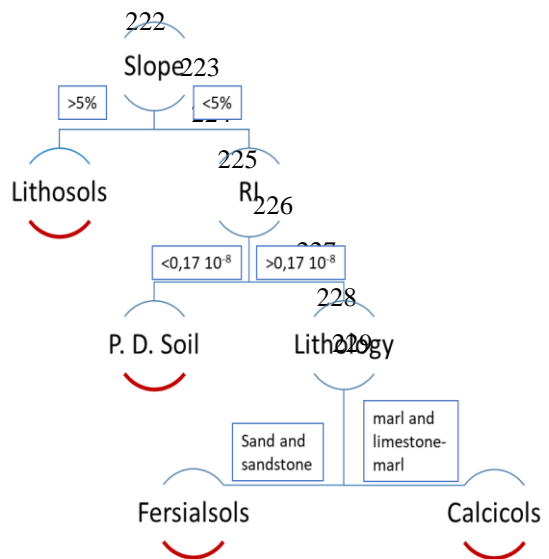
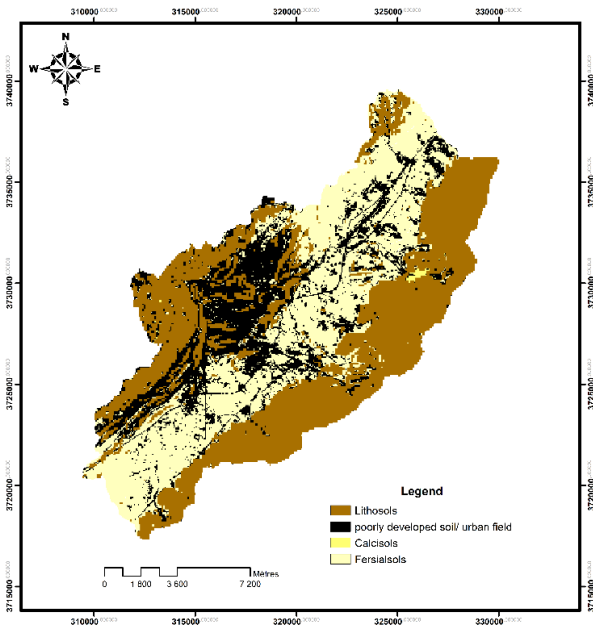


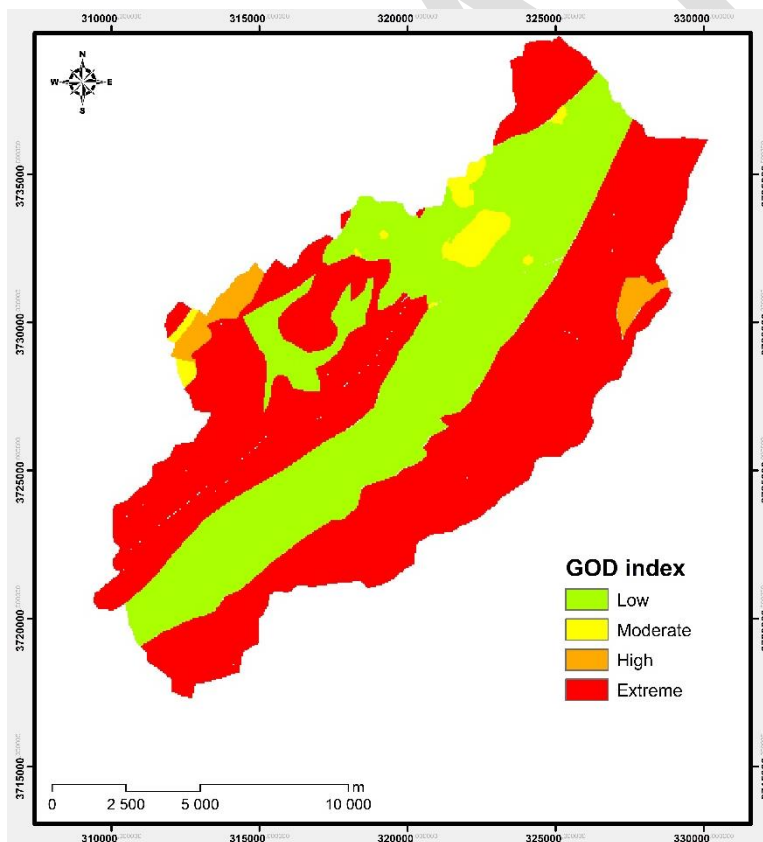
Fig. 11. Four classes resulting of DT



248

249

Fig. 12. DT map of study area



268

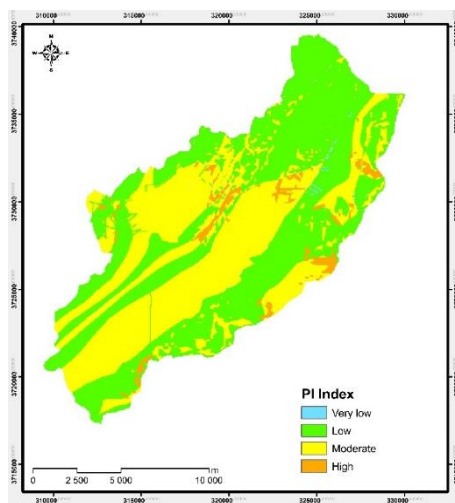
269

Fig. 13 Vulnerability map of GOD

270 3.4 PI map

271 Also, using and integrated different maps of RS processing: lithology, lineament and
 272 soil nature, in GIS database, allows to calculate Protection and Infiltration indexes. These
 273 layers served to mapping vulnerability using PI method. The final vulnerability map is
 274 depicted in figure 14. It shows four classes: very low to high vulnerability. It is noted that
 275 the moderate vulnerability occurs, principally in the middle of the watershed.

276



277

278 **Fig. 14. Vulnerability map of PI**

279 4 Discussion

280 The low values of NDVI indicate absence vegetation cover in study zone, which facilitates
 281 the interpretation of satellite images.

282 The main features that are usually visible by RS treatments are the lithological distribu-
 283 tions as well as the faults, shears and fractures. For that reason, band combination images
 284 for this study area were created to show the delimitation of outcrop limits for each image
 285 scene who was processed through creation of image stack (RGB and ratio):

286 Bands (7, 6 and 5) gave a false color image composite with an enhanced image with
 287 the rocky outcrops shown in shades of light purple and olive. The vegetation apparent on
 288 blue. Bands 7, 5 and 3 give the green shade to the clay-limestone formation and the purple
 289 to sandstone one. Last band (543) combination give the red nuance for agriculture area,
 290 and pink and gray for sandstone and claying outcrops. Accordingly, a band ratio color
 291 composite was prepared by assembling the ratios: (6/7, 6/4, 4/2), (6/7, 4/2, 5/4) and (7/6,

292 5/6, 2/4) in RGB, respectively. As it is clear from these images, the limit of formation is
293 more obvious that in band combination maps.

294 The directional filters used to mapping lineaments of the Deffa watershed, which is
295 perfectly overlap with geomorphological structures of study area. The lineament rose
296 shows the directional frequency of the mapped lineaments over the area of study. The
297 rose diagram of the detected lineaments show two prominent trends in the directions of
298 the N40° and N150°, which are also the principal directions of the regional structures in
299 Amour Mountains (Stamboul, 2005).

300 For pedology treatment, we used RI to identify the soil nature. The important values
301 coincided to the agricultural area. The low values indicate complete absence of soil or, in
302 our case urbanisation area. Set of parameters involve developing soil in arid zone, the
303 authors used frequently the topography, lithology and soil indexes (Color index, Bright-
304 ness index...) to predicted soil map (Kazi Tani, 2016; Ben-Dor et al, 2006, Zeraatpisheh
305 et al, 2018; Gray et al, 2016; Escadafal and Pouget, 1987). In our case, the DT was elab-
306 orated using the environmental covariates: slope, RI and lithology. The map resulted four
307 classes of different soil nature: Lithosols covered 42.67% of the area corresponding a
308 slope high than 5%. In the slightly sloping region, depending on the RI (lower values),
309 21% is occupied by poorly developed soil and urban filed. The rest of surface, the lithol-
310 ogy nature conditions shows existence of 35% Fersialsols and just 0.19% of Calcisols.

311

312 All the aforementioned information were compiled in a GIS database to map vulnera-
313 bility of groundwater in watershed of Deffa using GOD and PI methods. The resulting
314 maps clearly showed differences. More than 57% and 37 % of watershed surface present
315 Extreme and Low vulnerability in GOD map but the 53% of area has low index of PI and
316 43% for moderate vulnerability. Additionally, to analyse the spatial pattern of the vulner-
317 ability classes, it is possible to identify that there are controversial areas:

- 318
- Limits of watershed: while these areas are extremely vulnerable in GOD, they
319 are in the low, moderate and high classes in PI: In these areas, the lithology
320 nature and depth of water table increase GOD index, but many details taken by
321 PI method highlight and specified the many areas with different vulnerability.

- 322 • Center of watershed present low GOD index but moderate value of PI index:
323 this is because GOD uses depth to water table in vulnerability assessment,
324 whereas PI neglects this parameter. In depression the high depth to water table,
325 make them low vulnerable in GOD map. Contrary to PI map, the flat topogra-
326 phy, favorite infiltration of pollutant, so these zones are more vulnerable.

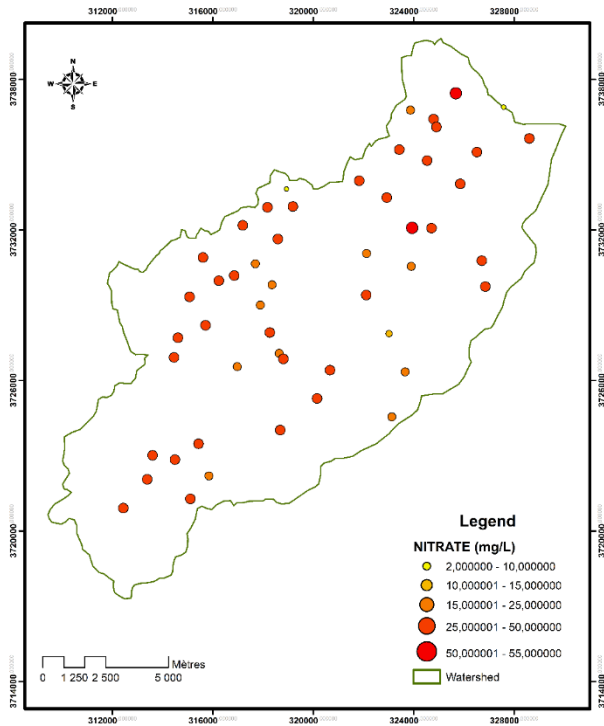
327 The natural nitrate concentration in groundwater under aerobic conditions is a few mil-
328 ligrams per liter (WHO, 2011), the study area presents concentrations between 3 and 55
329 mg/L. While 50 mg/L is considered very high concentration for drinking water.

330 The comparison of chemical concentration in groundwater samples of boreholes and
331 both of maps show that the average of NH_4^+ and SO_4^{2-} concentration in low class is higher
332 than extreme one for GOD map.

333 The Spatial distribution map of nitrate (fig. 15) showed that high concentrations of
334 NO_3^- is in the center of the basin coinciding with moderate and high PI index. Correlation
335 coefficient is one of the parameter useful in vulnerability map validation (Lake et al. 2003,
336 Kumar and Krishna, 2018; Mfumu Kihumba et al, 2017). The relationships between the
337 vulnerability indexes and NO_3^- concentration (fig. 16) show that PI index correlates neg-
338 atively with nitrate concentration. This means that high PI values, that represent a high
339 degree of natural protection and low vulnerability, correspond with lower values of ni-
340 trates, being consistent with the expectation. However, GOD index showed ???

341 Furthermore, the Spearman's rank correlation coefficient (Bonham-Carter, 1994) was
342 calculate for PI and GOD indexes; the values of -0.86 and 0.47 have been obtained re-
343 spectively, indicating that vulnerability map by PI approach matches to some extent aq-
344 uifer pollution state as expressed by the nitrate distribution in the groundwater.

345



347

348 **Fig. 15. Spatial repartition of NO₃⁻, used to validate of vulnerability maps**

349

350

351

352

353

354

355

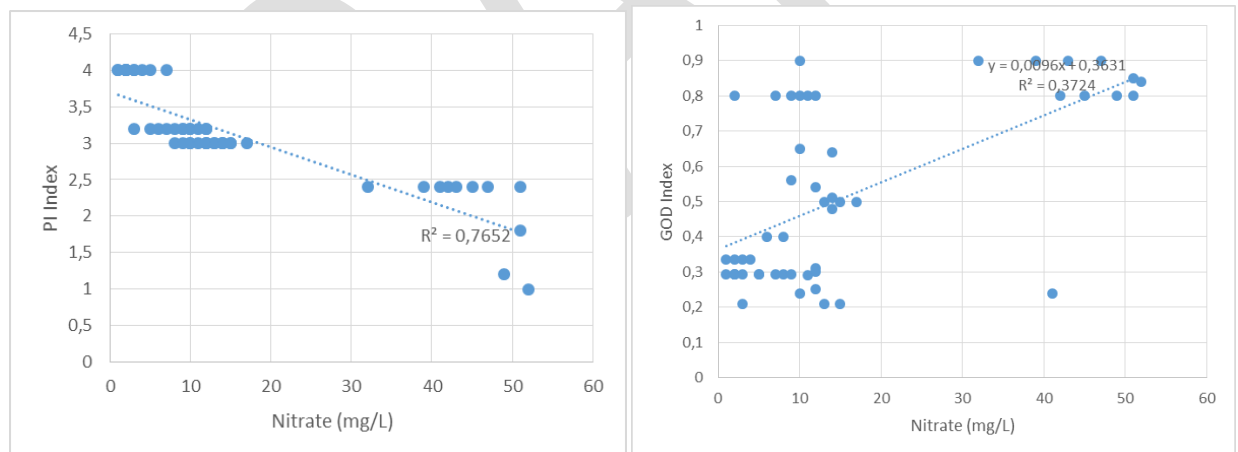
356

357

358

359

360



361

361 **Fig. 16. Correlation for PI and GOD Indexes by scatter plot.**

362

362 **5 Conclusions**

363

364

365

366

In this research, a combination of analysis techniques of spatial information were used to sensing vulnerability of Deffa catchment to pollution. The treatment of Landsat 8-OLI multi-spectral bands is presented. Based on the interpretation of RGB combinations of bands and ratios, and deferent filter, the geo-structural map was produced in big scale.

367 The other indexes were calculated (NDVI and RI) and involved in DT to mapping soil
368 nature. That help us to calculate GOD and PI index. The result of these map indicated
369 high to extreme vulnerability in big part of study region, however the comparison with
370 concentrations of pollutants in groundwater revealed that the PI approach suits Deffa
371 catchment more than GOD because GOD neglects important factors that affect vulnera-
372 bility in arid zone. These factors include topography, precipitation regime, fracturing, in
373 addition to soil nature.

374 The resulting vulnerability map can be used to delineate areas for groundwater protection
375 and management of land occupation

376 Many analysis technics can be applied to multispectral imagery to extract specific spa-
377 tial information. For this, it is important to make the best use of the merged techniques in
378 the development of groundwater resources.

379

380 **Data Availability:**

381 The satellite images that support the findings of this study are available online:
382 <https://landsat.usgs.gov/landsat-missions-timeline>.

383

384 **Acknowledgments:**

385 The authors are grateful to team of CEHIUMA, Málaga, for his kind support. We are
386 thankful to Mr. Tabti Nouredin, engineer at the DRE of Saida, Algeria. To Amadou
387 Taibou Issoufa, student in Tlemcen university, for his help. Our hearty thanks to the anon-
388 ymous reviewer and Editor-in-Chief for his valuable suggestions to improve the study in
389 the present form.

390

391 **References**

392 Beiranvand Pour A., Park Y., Park T.S., Hong J. K., Hashim M., Woo J., Ayoobi I.,
393 (2018): Regional geology mapping using satellite-based remote sensing ap-
394 proach in Northern Victoria Land, Antarctica, Polar Science, Volume 16,
395 Pages 23-46, ISSN 1873-9652, <https://doi.org/10.1016/j.polar.2018.02.004>.

396 B. E. T.G. H., Bureau d'études techniques de géologie et hydrogéologie, Geo-Water
397 (2003), Etude géologique et hydrogéologique du secteur EL Bayadh.

- 398 Ben-Dor E., Levin N., Singer A., Kamieli A., Braun O., Kidron G. J. (2006):
399 Quantitative mapping of the soil rubification process on sand dunes
400 using an airborne hyperspectral sensor. *Geoderma* 131, pp1-21.
- 401 Bentaher I., Raji M., (2021): Comparison of Landsat OLI, ASTER, and Sentinel 2A
402 data in lithological mapping : A Case study of Rich area (Central High Atlas,
403 Morocco), *Advances in Space Research*, Volume 67, Issue 3, Pages 945-963,
404 ISSN 0273-1177, <https://doi.org/10.1016/j.asr.2020.10.037>.
- 405 Bonham-Carter, G.F., (1994): *Geographical Information Systems for Geoscientists;*
406 *Modelling with GIS*, Pergamon, Kidlington.
- 407 Cornet A. (1952): L'Atlas Saharien Sud Oranais. XIX ème Congrès géologique in-
408 terne, Alger, Monographies régionales, 51 p, 9 fig, 1 pl.
- 409 Engle E.M., Harrison J.B.J., Hendrickx J.M.H., and Borchers B. (2010): Digital Soil
410 Boundary Detection Using Quantitative Hydrologic Remote Sensing. *Digital*
411 *Soil Mapping*, *Progress in Soil Science* 2, DOI 10.1007/978-90-481-8863-
412 5_11, C Springer Science+Business Media B.V.
- 413 Eldosouky M.A., Abdelkareem M., Elkhateeb O.S. (2017): Integration of remote sens-
414 ing and aeromagnetic data for mapping structural features and hydrothermal
415 alteration zones in Wadi Allaqi area, south eastern desert of Egypt, *J. Afr.*
416 *Earth Sci.*, 130, pp. 28-37.
- 417 Escadafal, R ; Pouget, M. (1987) : Cartographie des formations superficielles en zone
418 aride (Tunisie méridionale) avec Landsat TM, Vol 26, Num 4, pp 9-12.
- 419 Foster S. S. D. (1987): Fundamental concepts in aquifer vulnerability pollution risk
420 and protection strategy." *Proceedings of International Conference: Vulnera-*
421 *bility of Soil and Groundwater to Pollutants*. Noordwijk, The Netherlands.
- 422 Foster S., Hirata R., Gomes D., D'Elia M., Paris M. (2007): *Groundwater quality pro-*
423 *tection - a guide for water utilities, municipal authorities and environment*
424 *agencies (also in Spanish & Portuguese)*. The World Bank, Washington, D.C.
- 425 Foster, S. S. D. and Hirata R. (1988): *Groundwater pollution risk assessment: a meth-*
426 *odology using available data."* WHO-PAHO/HPECEPIS Technical Manual.
427 Lima, Peru.

- 428 Gabr S.S., Hassan S.M., Sadek M.F. (2015): Prospecting for new gold-bearing altera-
429 tion zones at El-Hoteib area, South Eastern Desert, Egypt, using remote sens-
430 ing data analysis, *Ore Geol. Rev.*, 71, pp. 1-13.
- 431 Ghazav R. and Ebrahim, Z. (2015): Assessing groundwater vulnerability to contami-
432 nation in an arid environment using DRASTIC and GOD models. *International Journal of Environmental Science and Technology*.
433 <http://dx.doi.org/10.1007/s13762-015-0813-2>.
- 434
- 435 Goldscheider N., Klute M., Sturm S., Hötzl H., (2000): The PI method – a GIS-
436 based approach to mapping groundwater vulnerability with special consid-
437 eration of karst aquifers. *Zeitschrift für angewandte Geologie*, 46, 3: 157-166
- 438 Goldscheider N. (2003): Karst groundwater vulnerability mapping: application of a
439 new method in the Swabian Alb. *Hydrogeol J* 13(4):555–564.
- 440 Gomes, C., Delacourt, C., Allemand, P., Ledru, P., and Wackerle, R. (2005): Using
441 Aster remote 393 sensing data set for geological mapping, in Namibia. *Physics and Chemistry of the Earth*, 394 Parts A/B/C, 30(1-3): 97-108.
- 442
- 443 Gray J. M., Bishop F.A. T., Wilfordc J. R. (2016): Lithology and soil relationships for
444 soil modelling and mapping. *Catena* 147, 429–440.
445 <http://dx.doi.org/10.1016/j.catena.2016.07.045>
- 446 Guerrero F. J. D. T, Hinojosa-Corona A., and Kretzsch T. G. (2016): A Comparative
447 Study of NDVI Values Between North- and South-Facing Slopes in a Semi-
448 arid Mountainous Region mar *IEEE Journal Of Selected Topics In Applied*
449 *Earth Observations And Remote Sensing*, vol. 9, no. 12, December.
- 450 Hash, S.J., (2008): Use of decision tree analysis for predictive soils mapping and im-
451 plementation on the Malheur County, Oregon initial soil survey. Masters The-
452 sis, Oregon State University, Corvallis. [https://doi.org/10.1016/S0098-](https://doi.org/10.1016/S0098-3004(99)00042-4)
453 [3004\(99\)00042-4](https://doi.org/10.1016/S0098-3004(99)00042-4).
- 454 Jensen, J. R., (1996): *Introductory to Digital Image Processing: A Remote Sensing*
455 *Perspective*, 2ed., Prentice-Hall, Englewood Cliffs, NJ.
- 456 Kazi Tani L., (2016): *Cartographie numérique des sols à l'échelle du paysage. Cas de*
457 *la région des Traras orientaux (Nord-Ouest de l'Algérie)*. PhD Thesis, Tlem-
458 cen University.

- 459 Kumar A. and Krishna A. P. (2018): Groundwater vulnerability and contamination
460 risk assessment using GIS-based modified DRASTIC-LU model in hard rock
461 aquifer system in India, Geocarto International, DOI:
462 10.1080/10106049.2018.1557259.
463 <https://doi.org/10.1080/10106049.2018.1557259>
- 464 Iain R Lake, Lovett A. L, Hiscock K.M., Betson M, Foley A., Sünnenberg G., Evers
465 S., Fletcher S., (2003): Evaluating factors influencing groundwater vulnera-
466 bility to nitrate pollution: developing the potential of GIS, Journal of Envi-
467 ronmental Management, Volume 68, Issue 3, Pages 315-328, ISSN 0301-
468 4797, [https://doi.org/10.1016/S0301-4797\(03\)00095-1](https://doi.org/10.1016/S0301-4797(03)00095-1).
- 469 Madeira J., (1993): Étude quantitative de relations constituantes minéralogiques. Ré-
470 flectance diffuse des latosols brésiliens. Ed. ORSTOM. Collection ÉTUDES
471 et THÈSES, Paris, 236p.
- 472 Martiny N., Camberlin P., Richard Y. & Philippon N. (2006): Compared regimes of
473 NDVI and rainfall in semi-arid regions of Africa, International Journal of Re-
474 mote Sensing, 27:23, 5201-5223, DOI: 10.1080/01431160600567787.
- 475 Mfumu Kihumba A., Vanclooster M., Ndembo Longo J., (2017): Assessing ground-
476 water vulnerability in the Kinshasa region, DR Congo, using a calibrated
477 DRASTIC model, Journal of African Earth Sciences, Volume 126, ,Pages 13-
478 22,ISSN 1464-343X, <https://doi.org/10.1016/j.jafrearsci.2016.11.025>.
- 479 Moonjun R., Farshad A., Shrestha D.P., and Vaiphasa C., (2010): Artificial Neural
480 Network and Decision Tree in Predictive Soil Mapping of Hoi Num Rin Sub-
481 Watershed, Thailand. J.L. Boettinger et al. (eds.), Digital Soil Mapping, Pro-
482 gress in Soil Science 2, DOI 10.1007/978-90-481-8863-5_11, C Springer Sci-
483 ence+Business Media B.V.
- 484 Pournamdary M., Hashim M., Pour B.A., (2014a): Application of ASTER and Landsat
485 TM data for geological mapping of Esfandagheh ophiolite complex, southern
486 Iran, Resour. Geol., 64 (3) , pp. 233-246
- 487 Pournamdary M., Hashim M., Pour B.A., (2014b): Spectral transformation of
488 ASTER and Landsat TM bands for lithological mapping of Soghan ophiolite
489 complex, south Iran Adv. Space Res., 54 (4) , pp. 694-709,

- 490 Qian, H., Li P., Howard, K.W.F., et al. , Chao Yang C., Zhang X., (2012): Assessment
491 of groundwater vulnerability in the Yinchuan Plain, Northwest China using
492 OREADIC. *Environ Monit Assess* 184, 3613–3628.
493 <https://doi.org/10.1007/s10661-011-2211-7>
- 494 Ridwan M. A., Radzi N. A. M. , Ahmad W. S. H. M. W. , Mustafa I. S. , Din N. M. ,
495 Jalil Y. E. , Isa A. M. , Othman N. S. , Zaki W. M. D. W., (2018): Applications
496 of Landsat-8 Data: a Survey. *International Journal of Engineering & Tech-*
497 *nology*, 7 (4.35), 436-441.
- 498 Saidi, S., Bouri, S., Dhia, H.B., (2011): Sensitivity analysis in groundwater vulnera-
499 bility assessment based on GIS in the Mahdia-Ksour Essaf aquifer, Tunisia:
500 a validation study. *Hydrological Sciences Journal – Journal des Sciences Hy-*
501 *drologiques* 56 (2), 288–304.
502 <https://doi.org/10.1080/02626667.2011.552886>.
- 503 Secund, S., Collin, M.L., Melloul, A.J., (1998): Groundwater vulnerability assessment
504 using a composite model combining DRASTIC with extensive agricultural
505 land use in Israel's Sharon region. *Journal of Environ. Management.* 54, 39–
506 57. <https://doi.org/10.1006/jema.1998.0221>.
- 507 Stamboul M. (2005): Contribution à l'étude hydrogéologique de l'Atlas saharien
508 l'exemple du Djebel Amour. PhD Theises, Univ. Oran, Algeria.
- 509 Thomas R. and Duraisamy V., (2018): Hydrogeological delineation of groundwater
510 vulnerability to droughts in semi-arid areas of western Ahmednagar district,
511 *The Egyptian Journal of Remote Sensing and Space Science*, Volume 21, Is-
512 sue 2, , Pages 121-137, ISSN 1110-9823,
513 <https://doi.org/10.1016/j.ejrs.2016.11.008>.
- 514
- 515 USGS, "Landsat Missions: Imaging the Earth Since 1972". (2019), Available online:
516 <https://landsat.usgs.gov/landsat-missions-timeline>, last visit: December 2019.
- 517 Van der Meer F.D., Van der Werff H.M.A., Van Ruitenbeek F.J.A., Hecker
518 C.A., Bakker W.H., Noomen M.F., Van der Meijde M., Carranza
519 E.J.M., Boudewijn de Smeth J., Woldai T., (2012): Multi- and hyperspectral

- 520 geologic remote sensing: a review *Int. J. Appl. Earth Obs. Geoinf.*, 2012 ,
521 pp. 112-128
- 522 World Health Organization (WHO) (2011): Nitrate and Nitrite in Drinking-Water;
523 Background Document for Development of WHO GUIDELINES for Drink-
524 ing-Water Quality; WHO: Geneva, Switzerland.
- 525 Yadav S.K., Borana S.L., (2019): Modis derived NDVI based time series analysis of
526 vegetation in the Jodhpur area. *The International Archives of the Photogram-*
527 *metry, Remote Sensing and Spatial Information Sciences*, Volume XLII-
528 3/W6, 2019 ISPRS-GEOGLAM-ISRS Joint Int. Workshop on “Earth Obser-
529 vations for Agricultural Monitoring”, 18–20 February 2019, New Delhi, In-
530 dia.
- 531 Zeraatpisheh M., Ayoubi S., Jafari A., Tajik S., Finke P., (2018): Digital mapping of
532 soil properties using multiple machine learning in a semi-arid region, central
533 Iran, *Geoderma*. Volume 338, 2019, Pages 445-452, ISSN 0016-
534 7061, <https://doi.org/10.1016/j.geoderma.2018.09.006>.
- 535
- 536 Zoheir B. and Emam A., (2012).: Integrating geologic and satellite imagery data for
537 high-resolution mapping and gold exploration targets in the south eastern de-
538 sert, Egypt *J. Afr. Earth Sci.*, 66–67 pp. 22-34.
- 539 Zumsprekel H., Prinz T., (2000): Computer-enhanced multispectral remote sensing
540 data: a useful tool for the geological mapping of Archean terrains in
541 (semi)arid environments, *Computers & Geosciences*, Volume 26, Issue 1,
542 2000, Pages 87-100, ISSN 0098-3004,